Measurement of forward $W \to e\nu$ production in pp collisions at $\sqrt{s} = 8\,\mathrm{TeV}$

The LHCb collaboration[†]

Abstract

A measurement of the cross-section for $W \to e\nu$ production in pp collisions is presented using data corresponding to an integrated luminosity of $2\,\mathrm{fb}^{-1}$ collected by the LHCb experiment at a centre-of-mass energy of $\sqrt{s} = 8\,\mathrm{TeV}$. The electrons are required to have more than $20\,\mathrm{GeV}$ of transverse momentum and to lie between 2.00 and 4.25 in pseudorapidity. The inclusive W production cross-sections, where the W decays to $e\nu$, are measured to be

$$\sigma_{W^+ \to e^+ \nu_e} = 1124.4 \pm 2.1 \pm 21.5 \pm 11.2 \pm 13.0\,\mathrm{pb},$$
$$\sigma_{W^- \to e^- \bar{\nu}_e} = 809.0 \pm 1.9 \pm 18.1 \pm 7.0 \pm 9.4\,\mathrm{pb},$$

where the first uncertainties are statistical, the second are systematic, the third are due to the knowledge of the LHC beam energy and the fourth are due to the luminosity determination. Differential cross-sections as a function of the electron pseudorapidity are measured. The W^+/W^- cross-section ratio and production charge asymmetry are also reported. Results are compared with theoretical predictions at next-to-next-to-leading order in perturbative quantum chromodynamics. Finally, in a precise test of lepton universality, the ratio of W boson branching fractions is determined to be

$$\mathcal{B}(W \to e\nu)/\mathcal{B}(W \to \mu\nu) = 1.020 \pm 0.002 \pm 0.019,$$

where the first uncertainty is statistical and the second is systematic.

[†]Authors are listed at the end of this paper.

1 Introduction

Precise measurements of the production cross-sections for W and Z bosons are important tests of the quantum chromodynamic (QCD) and electroweak (EW) sectors of the Standard Model (SM). In addition, the parton distribution functions (PDFs) of the proton can be better constrained [1]. The production of EW bosons has therefore been an important benchmark process to measure at current and past colliders. Measurements performed by the ATLAS [2–4], CMS [5–7], and LHCb [8–14] collaborations are in good agreement with theoretical predictions that are determined from parton-parton cross-sections convolved with PDFs. The precision of these predictions is limited by the accuracy of the PDFs and by unknown QCD corrections which are beyond next-to-next-to-leading order (NNLO) in perturbative QCD [15, 16].

The PDFs, as functions of the Bjorken-x values of the partons, have significant uncertainties at very low and large momentum fractions. Since the Bjorken-x values of the interacting partons, x_a and x_b, are related to the boson through its rapidity, $y = \frac{1}{2} \ln \frac{x_a}{x_b}$, forward measurements of production cross-sections are particularly valuable in constraining PDFs. The LHCb detector, which is instrumented in the forward region, is in a unique situation to provide input on determining accurate PDFs at small and large Bjorken-x values. At large rapidities the measurements are mainly sensitive to scattering between valence and sea quarks, while at low rapidities scattering between pairs of sea quarks also contributes significantly. The W^+/W^- cross-section ratio and the production charge asymmetry of the W boson are primarily sensitive to the ratio of u- and d-quark densities. In addition, the cross-section ratio and charge asymmetry enable the SM to be tested to greater precision since experimental and theoretical uncertainties partially cancel.

Here, the W production cross-section is measured in the electron[1] final state. Compared to muons, the measurement of electrons has an additional experimental difficulty arising from the bremsstrahlung emitted when traversing the detector material. While the emitted photon energy can often be recovered for low-energy particles, electrons from W boson decays tend to have high momentum, with bremsstrahlung photons that are not generally well-separated from the lepton. Coupled with the fact that individual LHCb calorimeter cells saturate by design at a transverse energy of approximately $10 \, \text{GeV}$, this leads to a poor energy measurement and a reconstructed distribution of transverse momentum, p_{T}^e, which differs significantly from the true transverse momentum of the electrons. In contrast, the electron direction is measured well, so that the differential cross-section in lepton pseudorapidity has negligible bin-to-bin migrations.

This paper presents measurements of the $W \rightarrow e\nu$ cross-sections[2], cross-section ratios, and the charge asymmetry at $\sqrt{s} = 8 \, \text{TeV}$ using data corresponding to an integrated luminosity of $2 \, \text{fb}^{-1}$ collected by the LHCb detector. Measurements are made in eight bins of lepton pseudorapidity. The electrons are required to have more than $20 \, \text{GeV}$ of transverse momentum[3] and to lie between 2.00 and 4.25 in pseudorapidity. The results are corrected for quantum electrodynamic (QED) final-state radiation (hereinafter denoted as "Born level"). These requirements define the fiducial region of the measurements.

---

[1]When referred to generically, "electron" denotes both e^+ and e^-.

[2]The decay $W \rightarrow e\nu$ denotes both $W^+ \rightarrow e^+\nu_e$ and $W^- \rightarrow e^-\overline{\nu}_e$ and similarly for the other leptonic decays. The $W \rightarrow e\nu$ cross-section denotes the product of the cross-section for W boson production and the branching fraction for $W \rightarrow e\nu$ decay.

[3]Natural units with $\hbar = c = 1$ are used throughout.

2 Detector and simulation

The LHCb detector [17, 18] is a single-arm forward spectrometer designed for the study of particles containing b or c quarks. The detector includes a high-precision tracking system consisting of a silicon-strip vertex detector surrounding the pp interaction region, a large-area silicon-strip detector located upstream of a dipole magnet with a bending power of about $4\,\mathrm{Tm}$, and three stations of silicon-strip detectors and straw drift tubes placed downstream of the magnet. The tracking system provides a measurement of momentum, p, of charged particles with a relative uncertainty that varies from 0.5% at low momentum to 1.0% at $200\,\mathrm{GeV}$. The minimum distance of a track to a primary vertex (PV), the impact parameter (IP), is measured with a resolution of $(15 + 29/p_\mathrm{T})\,\mathrm{\mu m}$, where p_T is the component of the momentum transverse to the beam, in GeV. Photons, electrons and hadrons are identified by a calorimeter system consisting of scintillating-pad (SPD) and preshower detectors (PRS), an electromagnetic calorimeter (ECAL) and a hadronic calorimeter (HCAL). The online event selection is performed by a trigger, which consists of a hardware stage, based on information from the calorimeter and muon systems, followed by a software stage, which applies a full event reconstruction. A set of global event cuts (GEC) is applied, which prevents events with high occupancy dominating the processing time of the software trigger.

Simulated data are used to optimise the event selection, estimate the background contamination and determine some efficiencies. In the simulation, pp collisions are generated using PYTHIA 8 [19] with a specific LHCb configuration [20]. The interaction of the generated particles with the detector, and its response, are implemented using the GEANT4 toolkit [21] as described in Ref. [22]. The momentum distribution of the partons inside the proton is parameterised by the leading-order CTEQ6L1 [23] PDF set. Final-state radiation (FSR) of the outgoing leptons is simulated using the model implemented internally within PYTHIA 8 [24].

3 Event selection

The production of $W \to e\nu$ is characterised by a single, isolated high-p_T charged particle originating from a PV with a large energy deposit in the electromagnetic calorimeter. However, several other physics processes can mimic this experimental signature. Significant EW backgrounds include $Z \to ee$ with one electron in the LHCb acceptance,[4] and $Z \to \tau\tau$ and $W \to \tau\nu$, where the τ decays to a final state containing an electron. Prompt photon production in association with jets contributes in cases where the photon converts to an ee pair and only one electron is reconstructed and selected. Hadronic backgrounds stem from four sources: hadron misidentification (hereinafter denoted as "fake electrons"), semileptonic heavy flavour decay, decay in flight, and $t\bar{t}$ production.

The event selection requires the electron candidate to satisfy the trigger at both hardware and software levels. The reconstructed electron candidates should have pseudorapidity, η^e, between 2.00 and 4.25, have p_T^e in excess of $20\,\mathrm{GeV}$ and should satisfy stringent track quality criteria. In particular, the relative uncertainty on the momentum is required to be less than 10% to ensure that the charge is measured well. The upper limit of $\eta^e < 4.25$ is imposed due to the limited acceptance of the calorimetry. To be

---

[4]Z denotes the combined Z and virtual photon (γ^*) contribution.

identified as electrons, the candidates are required to deposit energy $E_{\mathrm{ECAL}} > 0.15p^e$ in the ECAL while depositing relatively little energy $E_{\mathrm{HCAL}} < 0.0075p^e$ in the HCAL, where p^e is the momentum of the electron. The candidates are also required to have deposited energy of more than 50 MeV in the PRS. The background formed by $Z \to ee$ events with both electrons in the LHCb acceptance is largely removed using a dedicated dielectron software trigger.

The remainder of the selection exploits other physical features of the process. Electrons from the W boson decay are prompt, in contrast to leptons that come from decays of heavy flavour mesons or τ leptons. Hence the IP is required to be less than 0.04 mm. Another discriminant against hadronic processes is the fact that electrons from the W boson tend to be isolated. On the other hand, leptons originating from hadronic decays, or fake electrons, tend to have hadrons travelling alongside them. The isolation requirement is set to be $I_{\mathrm{T}}^e > 0.9$, where I_{T}^e is defined as

$$I_{\mathrm{T}}^e \equiv \frac{p_{\mathrm{T}}^e}{p_{\mathrm{T}}^e + E_{\mathrm{T}}^{\gamma} + p_{\mathrm{T}}^{\mathrm{ch}}}. \tag{1}$$

Here E_{T}^{γ} is the sum of the transverse component of neutral energy in the annular cone with $0.1 < R < 0.5$, where $R \equiv \sqrt{\Delta\eta^2 + \Delta\phi^2}$ and $\Delta\eta$ and $\Delta\phi$ are the differences in the pseudorapidity and azimuthal angle between the candidate and the particle being considered, and $p_{\mathrm{T}}^{\mathrm{ch}}$ is the scalar sum of the transverse momenta of charged tracks in the same annular cone. Bremsstrahlung photons are mostly contained in the range $0.0 < R < 0.1$ and so are excluded from the isolation requirement.

4 Signal yield

In total, $1\,368\,539$ $W \to e\nu$ candidates fulfil the selection requirements. The signal yields are determined in eight bins of lepton pseudorapidity and for each charge. Binned maximum likelihood template fits to the p_{T} distribution of the electron candidate are performed in the range $20 < p_{\mathrm{T}}^e < 65$ GeV, following Ref. [25]. The p_{T}^e spectra in the 16 bins of pseudorapidity and charge with the results of the fits superimposed are reported in Appendix C.

Templates for $W \to e\nu$, $W \to \tau\nu$, $Z \to ee$ and $Z \to \tau\tau \to eX$ are taken from simulation, where X represents any additional particles. The known ratio of branching fractions [26] is used to constrain the ratio of $W \to \tau\nu$ to $W \to e\nu$. The measured LHCb cross-section for $Z \to \mu\mu$ production [9] is used to constrain $Z \to ee$ and $Z \to \tau\tau \to eX$ in the fit, and knowledge of the ratio of branching fractions to different leptonic final states of the Z boson [26] is also taken into account.

Contributions from $W\gamma$, $Z\gamma$, WW, WZ, and $t\bar{t}$ events are included in the fits. These processes account for $(0.46 \pm 0.01)\%$ of the selected candidates and are denoted as "rare processes" in the following. The templates for these processes are obtained from simulation and normalised to the MCFM [27] NLO cross-section predictions.

The production of prompt photons in association with jets has a cross-section of about 50 nb for a $p_{\mathrm{T}} > 20$ GeV photon within the LHCb acceptance, as computed using MCFM at NLO. This process mimics the signal in cases where the photon converts into an ee pair in the detector material and one electron satisfies the $W \to e\nu$ selection. A sample of photon+jets candidates is obtained from data by searching for an ee pair with mass

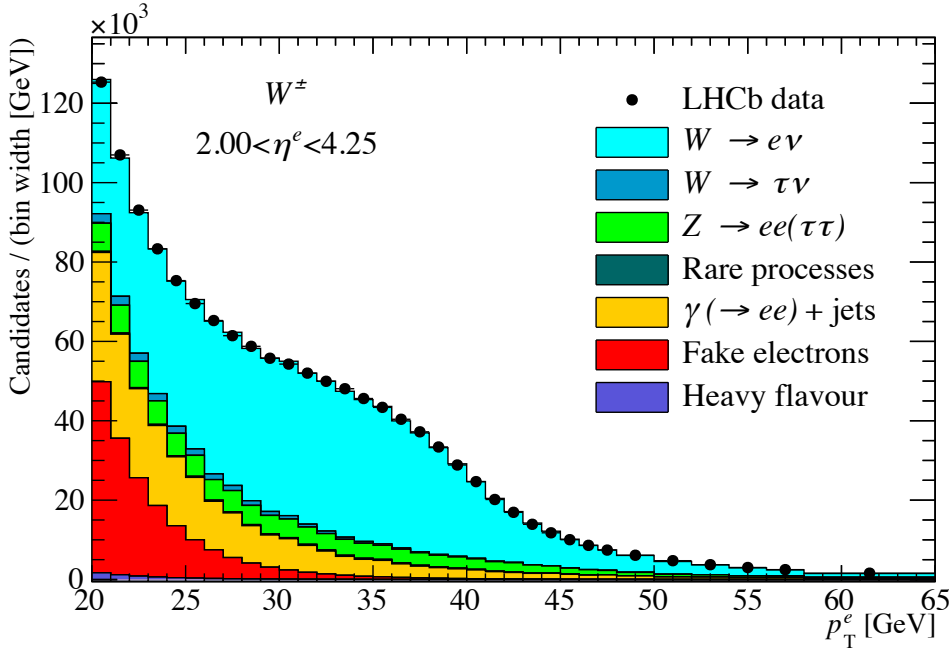Figure 1: The inclusive fit to the p_{T}^e distribution of the full dataset. The χ^2/ndf of the fit is 1.1 with 33 degrees of freedom.

below $50\,\mathrm{MeV}$ and applying stringent selection criteria to the candidates. Simulation is used to account for the differences in the $W \rightarrow e\nu$ and $\gamma \rightarrow ee$ selections.

Hadron misidentification occurs when hadrons begin to shower early in the ECAL, giving a shower profile similar to that of electrons. These hadrons, however, will tend to deposit fractionally more energy in the HCAL than genuine electrons and will also be less isolated on average. A template for the p_{T} distribution of fake electrons is determined using data, by modifying the isolation and HCAL energy requirements of the selection to produce a sample dominated by hadrons.

The semileptonic decay of heavy flavour (HF) hadrons gives rise to genuine electrons. This background is suppressed using the IP requirement to exploit the long lifetimes of hadrons containing b and c quarks. The remaining HF component is described by a data-driven template obtained by applying the standard selection but requiring the impact parameter to be significantly different from zero. The normalisation of the remaining contribution in the fit to p_{T}^e is determined from a separate template fit to the χ^2_{IP} distribution, where χ^2_{IP} is the difference between the χ^2 of the PV fit when reconstructed with and without the candidate electron. The fractional HF component in the signal region is determined to be smaller than 0.8% at 68% confidence level.

The $W \rightarrow (e, \tau)\nu_{(e,\tau)}$ and fake electron fractions are free to vary in the fits, while the remaining components are constrained as described previously. The validity of the SM is implicitly assumed in the constraints based on theoretical cross-sections obtained from MCFM and in extracting template shapes from simulation. The $W^+ \rightarrow e^+\nu_e$ and $W^- \rightarrow e^-\overline{\nu}_e$ sample purities are determined to be $(63.95 \pm 0.19)\%$ and $(56.06 \pm 0.21)\%$. The p_{T}^e distribution of the full dataset with the result of the fit overlaid is shown for illustration in Fig. 1 and is used in the estimation of systematic uncertainties.

5 Cross-section measurement

The production cross-section for $W \to e\nu$ is measured in each bin of lepton pseudorapidity and for each charge with electron transverse momentum in excess of $20\,\mathrm{GeV}$. The cross-section is determined from

$$\sigma_i^{W \to e\nu} = \frac{N_i^W}{\mathcal{A}_i \, L \, \epsilon_i^{\mathrm{tot}} \, f^{\mathrm{FSR}}}, \tag{2}$$

where N_i^W is the signal yield in the range $20 < p_{\mathrm{T}}^e < 65\,\mathrm{GeV}$ obtained from the fit in bin i of η^e, $\epsilon_i^{\mathrm{tot}}$ is the total efficiency in that bin, and L is the integrated luminosity. The signal yields are corrected for excluded candidates with $p_{\mathrm{T}}^e > 65\,\mathrm{GeV}$ by computing a charge-dependent acceptance factor, $\mathcal{A}_i$, using a RESBOS [28–30] simulation.

The results of the measurement are quoted at Born level to enable comparisons to theoretical predictions that do not incorporate the effect of QED final-state radiation. Correcting to Born level also enables a comparison to be made with the measurement of $W \to \mu\nu$. Corrections due to FSR, f^{FSR}, are computed separately using PYTHIA 8 and HERWIG++ [31] and then averaged. The corrections are listed in Appendix A so that the measurement can be compared to a prediction that incorporates the effect of FSR.

The total efficiency used to correct the candidate yield can be written as the product

$$\epsilon^{\mathrm{tot}} \equiv \epsilon^{\mathrm{track}} \cdot \epsilon^{\mathrm{kin}} \cdot \epsilon^{\mathrm{PID}} \cdot \epsilon^{\mathrm{GEC}} \cdot \epsilon^{\mathrm{trigger}} \cdot \epsilon^{\mathrm{tight}}. \tag{3}$$

The description and estimation of the various terms are explained below. Each subsequent efficiency is determined in a subset of events defined by the preceding requirements in order to ensure that correlations between the requirements are correctly accounted for.

The track reconstruction efficiency, $\epsilon^{\mathrm{track}}$, is the probability that an electron is reconstructed as a track satisfying standard track quality criteria and the requirement that the relative momentum uncertainty is less than 10%. The efficiency is determined using simulation of $W \to e\nu$ and cross-checked with a data-driven study using $Z \to ee$ candidate events [12].

An electron with true p_{T} of more than $20\,\mathrm{GeV}$ can be reconstructed as having $p_{\mathrm{T}}^e < 20\,\mathrm{GeV}$. This is predominantly due to bremsstrahlung. For high-p_{T} candidates, the photons tend to lie close to the electron and are often not correctly identified by bremsstrahlung recovery. The correction for this effect, ϵ^{kin}, is determined using simulation and is cross-checked in data using the method outlined in Ref. [12].

Simulation of $W \to e\nu$ is used to extract an efficiency, ϵ^{PID}, for the loose particle identification (PID) requirements that are applied in the initial selection of electron candidates. The efficiency is corrected using the data-driven technique employed for $Z \to ee$ candidate events [12].

The hardware trigger incorporates a global event cut (GEC) on the number of SPD hits, $N_{\mathrm{SPD}} < 600$, to prevent high-multiplicity events from dominating the processing time at trigger-level. Dimuon events have a less stringent requirement of $N_{\mathrm{SPD}} < 900$ and are used to determine the fraction of events, ϵ^{GEC}, below $N_{\mathrm{SPD}} = 600$. However, dimuon candidate events are not entirely comparable to $W \to e\nu$ as electrons will shower in the detector and lead to more hits in the SPD. Nevertheless, after a suitable shift of the dimuon distribution, good agreement is observed with $W \to e\nu$ candidate events.

A tag-and-probe method [12] is used on $Z \to ee$ data to determine the efficiency, $\epsilon^{\mathrm{trigger}}$, for the single-electron triggers. The tag is an electron from a Z candidate that satisfies

Table 1: Summary of the relative uncertainties on the W^+ and W^- boson cross-sections and on the cross-section ratio. Uncertainties marked with † are assumed to be uncorrelated between bins; all others are taken to be correlated.

Source	Uncertainty [%]		
	$\sigma_{W^+\to e^+\nu_e}$	$\sigma_{W^-\to e^-\bar{\nu}_e}$	$R_{W^\pm}$
Statistical†	0.19	0.24	0.30
Yield (statistical)†	0.28	0.40	0.48
Yield (systematic)	1.42	1.79	0.51
Efficiency (statistical)†	0.55	0.55	0.21
Efficiency (systematic)	1.11	1.14	0.54
FSR corrections†	0.05	0.07	0.09
Acceptance corrections (statistical)†	0.00	0.01	0.01
Acceptance corrections (systematic)	0.15	0.15	0.00
Charge mis-identification†	—	—	0.02
Systematic	1.91	2.23	0.91
Beam energy	1.00	0.86	0.14
Luminosity	1.16	1.16	—
Total	2.46	2.67	0.97

the above requirements and meets all trigger requirements. The probe is then used to determine the fraction of candidates that satisfy the trigger requirements. The hadronic background in the $Z \to ee$ dataset is estimated using same-sign, $e^\pm e^\pm$, events. The efficiency for a veto on the dielectron trigger is determined using simulation of $W \to e\nu$ and is close to 100%.

Tight selection requirements consist of more stringent track quality requirements and PID requirements, as well as ensuring the track is prompt and isolated. The efficiency for these requirements, ϵ^{tight}, is determined using Z data analogously to the procedure for determining the trigger efficiency.

Efficiencies determined from $Z \to ee$ cannot be directly used for W production due to the different couplings at the production and decay vertices, a different mixture of interacting quarks, and, most importantly, the difference in mass. This results in a p_{T}^e distribution that is harder for electrons from the Z boson. Consequently, efficiencies that show a dependence on p_{T}^e are liable to be biased. This is corrected for in each bin of η^e using W and Z simulation.

6 Systematic uncertainties

Several sources of systematic uncertainty affect the measurement. These are summarised in Table 1 for the total cross-sections in the fiducial region and the ratio measurements where $R_{W^\pm} \equiv \sigma_{W^+\to e^+\nu_e}/\sigma_{W^-\to e^-\bar{\nu}_e}$.

The yields determined from fits to the p_{T}^e distribution are affected by two types of uncertainty. The effect of the statistical uncertainty in the templates is evaluated using pseudoexperiments and is denoted as "Yield (statistical)" in Table 1. All other sources of uncertainty in the fits are considered systematic in nature (denoted as "Yield (systematic)"

in Table 1) and are described in the next paragraph.

Templates for contributions from photon+jets, fake electrons and heavy flavours, determined using data, contain a mixture of physical processes. A simulation-based estimate for EW contamination is subtracted and a 50% systematic uncertainty is assigned for the procedure. Components that are constrained in the fits are varied according to their respective uncertainties. Templates for $Z \to ee$ and $Z \to \tau\tau \to eX$ are subject to an uncertainty on the cross-section, and the normalisation of the rare processes has an uncertainty from the cross-sections and the luminosity determination. Two alternative control regions are considered for determining the fake electron component resulting in an uncertainty of 0.6% on the total cross-section. The fits are repeated with these alternative regions to ascertain the uncertainty associated with the fake electron template. The systematic uncertainty on the normalisation of the heavy flavour component is 0.8% and the data-driven p_{T} template is varied accordingly. The transverse momentum of the candidate in simulation is sensitive to both the potential mismodelling of track reconstruction and the description of the material traversed by the candidate. The latter affects the number of bremsstrahlung photons emitted and thus has an impact on the p_{T}^e of the candidate and, by extension, on the fits. Any potential mismodelling can be described by a scaling of the momentum, as explained in Ref. [12]. The effect of varying the momentum scale on all simulation-based templates is tested on the inclusive fit shown in Fig. 1 and the best fit value for the momentum scale is seen to be consistent with unity, suggesting that material in the detector is modelled well. An uncertainty of 0.5% assigned on the momentum scale in Ref. [12] is found to be appropriate for the measurement. Varying the momentum scale by its uncertainty in the fits binned in η^e leads to an uncertainty of 1.3% on the total cross-section which is the largest contribution to "Yield (systematic)".

The statistical uncertainty on the total efficiency is taken as a contribution to the uncertainty on the measurement and is denoted as "Efficiency (statistical)" in Table 1. In the case of cross-sections, the uncertainties from the finite statistics of the Z data and Z/W simulated samples all contribute. For the determination of the cross-section ratio and the charge asymmetry, only the uncertainty due to the simulation of the W must be accounted for. All other sources of uncertainty in the efficiencies are collectively denoted as "Efficiency (systematic)" in Table 1 and are described in the next paragraph.

Data-driven cross-checks performed on the efficiencies determined using simulation lead to an uncertainty of 0.5% on the track reconstruction efficiency, an uncertainty of 0.6% on the kinematic efficiency due to the modelling of bremsstrahlung in simulation, and an uncertainty of 0.6% on PID requirements. The statistical component of the uncertainty on the GEC efficiency is found to be 0.09%. Since ϵ^{GEC} is dependent on the number of primary vertices, N_{PV}, the efficiency is measured separately for $N_{\mathrm{PV}} = \{1, 2, 3, \geq 4\}$ and combined. This is compared with the estimate of the efficiency obtained inclusively for all numbers of primary vertices and an uncertainty of 0.33% is assigned based on the difference between the two methods. Overall, a systematic uncertainty of 0.34% is assigned for the procedure to determine the efficiency from dimuon candidate events. An additional systematic uncertainty is assigned on the cross-sections, the cross-section ratio, and the charge asymmetry to account for the differences observed between electrons and positrons in simulation. Same-sign subtraction is performed when the $Z \to ee$ data sample is used. A study that formed electron and charged pion combinations and counted opposite- and same-sign pairs [12] leads to a systematic uncertainty of 0.25% on the

7

$W \to e\nu$ cross-section due to the normalisation of hadronic contamination in the sample of $Z \to ee$ candidates.

Half the difference between PYTHIA 8 and HERWIG++ predictions is taken as the systematic component of the uncertainty on FSR corrections.

The statistical uncertainty on the acceptance corrections arises from the RESBOS W simulated sample. Half the difference between PYTHIA 8 and RESBOS is taken as a systematic uncertainty on a bin-by-bin basis and is assumed to be correlated between bins.

A small fraction of candidate electrons have the wrong charge assigned to them, which leads to a bias in the cross-section ratio and the charge asymmetry. A correction of $(0.58 \pm 0.05)\%$ is determined using simulation and applied to the measurements.

The uncertainty on the LHC beam energy at $8\,\mathrm{TeV}$ [32] leads to a relative uncertainty on the W^+ (W^-) cross-section of $1.00\,(0.86)\%$ determined using DYNNLO [33]. The uncertainty on the luminosity is 1.16% for the $8\,\mathrm{TeV}$ dataset [34].

7   Results

7.1   Propagation of uncertainties

When computing derived quantities such as the total cross-section, cross-section ratios, and the charge asymmetry, correlations between the 16 measurements of $W \to e\nu$ in bins of η^e must be accounted for. Uncertainties marked with † in Table 1 are statistical in nature and are assumed to be uncorrelated between charges and bins of η^e. All other sources of systematic uncertainty are varied by one standard deviation around their nominal value for each measurement and the correlation between each pair of measurements is computed. Correlation matrices between bins of η^e for W^+, W^-, and W^+ against W^- are reported in Appendix B. A consequence of the sizeable positive correlations is that many of the systematic uncertainties add coherently when integrating over bins, but partially cancel in determining W^+/W^- ratios.

Sect. 7.5 presents the ratio of the $W \to e\nu$ and $W \to \mu\nu$ branching fractions. Here, the systematic uncertainties of the respective measurements are taken to be uncorrelated between the two final states apart from the uncertainties on the GEC efficiency and the acceptance correction, which are taken to be fully correlated.

7.2   Inclusive results

Total inclusive cross-sections for $W \to e\nu$ production are obtained by summing the cross-sections in bins of η^e. The Born level cross-sections in the fiducial region defined as $2.0 < \eta^e < 4.25$ and more than $20\,\mathrm{GeV}$ of transverse momentum are measured to be

$$\sigma_{W^+ \to e^+\nu_e} = 1124.4 \pm 2.1 \pm 21.5 \pm 11.2 \pm 13.0\,\mathrm{pb},$$
$$\sigma_{W^- \to e^-\overline{\nu}_e} = 809.0 \pm 1.9 \pm 18.1 \pm 7.0 \pm 9.4\,\mathrm{pb},$$
$$\sigma_{W \to e\nu} = 1933.3 \pm 2.9 \pm 38.2 \pm 18.2 \pm 22.4\,\mathrm{pb},$$

where the first uncertainties are statistical, the second are systematic, the third are due to the knowledge of the LHC beam energy and the fourth are due to the luminosity determination.
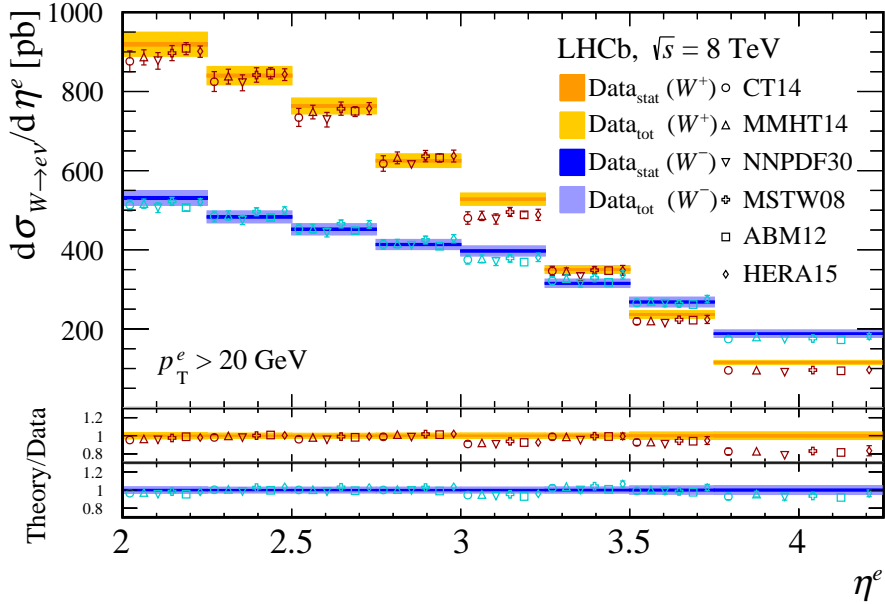
Figure 2: The differential W^+ and W^- cross-sections in bins of η^e. Measurements, represented as bands, are compared to NNLO predictions with different parameterisations of the PDFs (markers are displaced horizontally for presentation). The bottom panel displays the theory predictions divided by the measured cross-sections.

The W^+ to W^- cross-section ratio is determined to be

$$R_{W^\pm} = 1.390 \pm 0.004 \pm 0.013 \pm 0.002,$$

where uncertainties are statistical, systematic and due to the LHC beam energy measurement, respectively.

7.3 Cross-sections as a function of electron pseudorapidity

Born level cross-sections as a function of electron pseudorapidity are tabulated in Appendix A. The differential cross-sections as a function of η^e are also determined and shown in Fig. 2. Measurements are compared to theoretical predictions calculated with the FEWZ [15, 16] generator at NNLO for the six PDF sets: ABM12 [35], CT14 [36], HERA1.5 [37], MMHT14 [38], MSTW08 [39], and NNPDF3.0 [40]. Satisfactory agreement is observed apart from in the far forward region of the W^+ differential measurement, where the PDF uncertainties are also greatest.
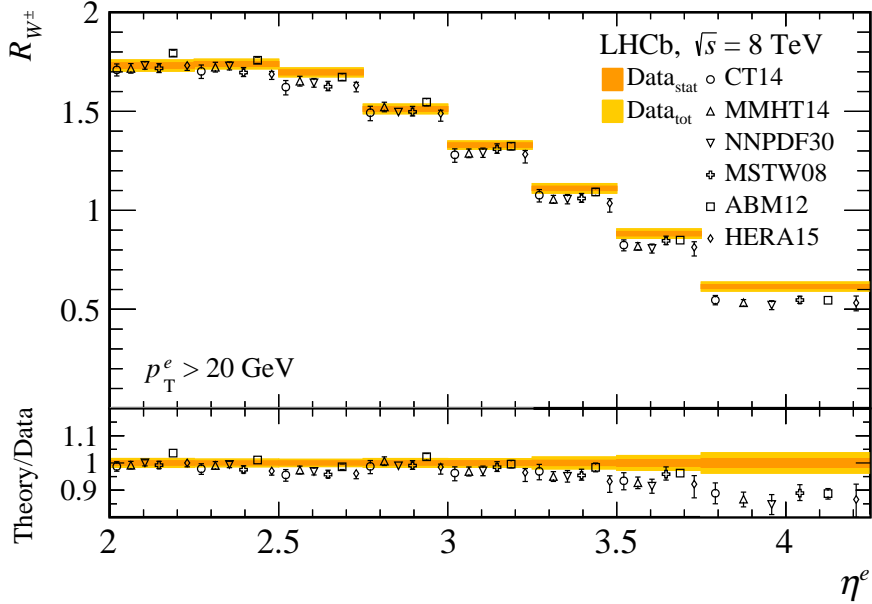
Figure 3: The W^+ to W^- cross-section ratio in bins of η^e. Measurements, represented as bands, are compared to NNLO predictions with different parameterisations of the PDFs (markers are displaced horizontally for presentation). The bottom panel displays the theory predictions divided by the measured cross-section ratios.

7.4 Cross-section ratio and charge asymmetry

Cross-section ratios as a function of η^e are compared to theory predictions in Fig. 3 and the measurements are tabulated in Appendix A. Overall the measurements are in agreement with theory predictions, with the exception of the far forward region. In this region the measured ratio is higher than the expectation as a consequence of the discrepancy seen in the W^+ cross-section in that region.

The W boson production charge asymmetry is defined as

$$A_e \equiv \frac{\sigma_{W^+ \to e^+ \nu_e} - \sigma_{W^- \to e^- \bar{\nu}_e}}{\sigma_{W^+ \to e^+ \nu_e} + \sigma_{W^- \to e^- \bar{\nu}_e}}. \tag{4}$$

The asymmetry is compared to theory predictions in bins of η^e in Fig. 4. The measurements are tabulated in Appendix A.

7.5 Lepton universality

Production of W bosons in the forward region has also been studied in the muon final state [9]. The muon measurement had a different upper kinematic limit in pseudorapidity, and consequently the bin boundaries only coincide with the present measurement for $\eta^l < 3.50$. The results are therefore compared in the range $2.00 < \eta^l < 3.50$ as is shown in Figs. 5, 6, and 7. The results of these measurements are seen to be consistent with the $W \to \mu\nu$ measurements and no significant deviation from lepton universality is observed once uncertainties and correlations between measurements are taken into account. Fig. 5 shows good agreement, apart from the bin $3.00 < \eta^l < 3.25$ for W^+, where the difference is approximately 3 standard deviations.
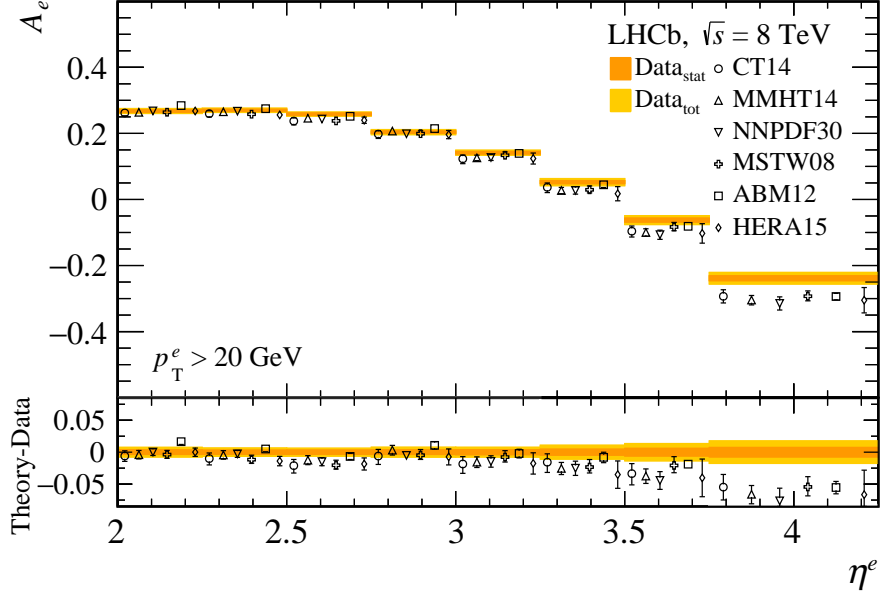
10

Figure 4: The W boson production charge asymmetry in bins of η^e. Measurements, represented as bands, are compared to NNLO predictions with different parameterisations of the PDFs (markers are displaced horizontally for presentation). The bottom panel displays the difference between theory predictions and the measured charge asymmetry.
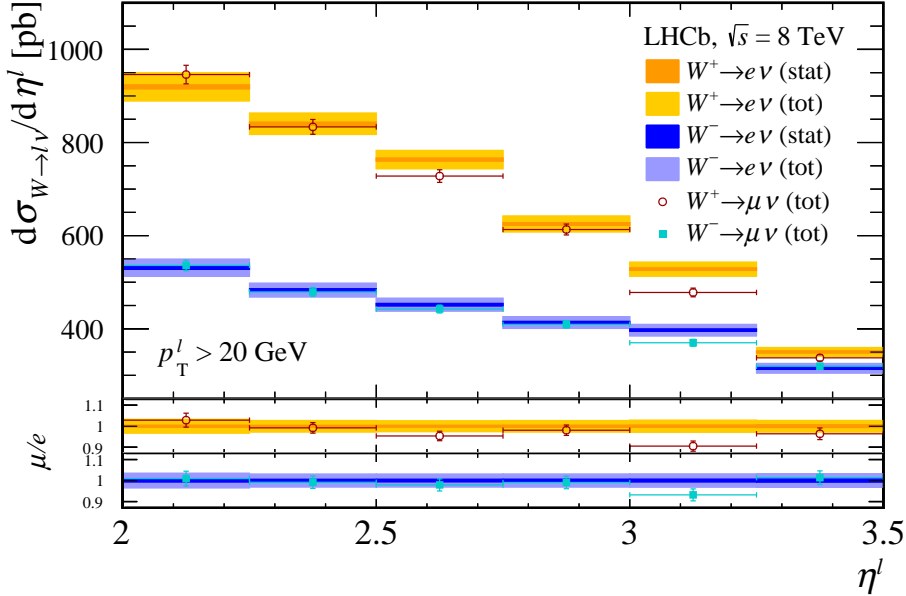

Figure 5: The differential W^+ and W^- cross-sections in bins of η^l. The measurement using electrons, represented as bands, is compared to the measurement in the muon final state. The bottom panel displays the muon results divided by the measurements in the electron final state.

Figure 6: The W^+ to W^- cross-section ratio in bins of η^l. The measurement using electrons, represented as bands, is compared to the measurement in the muon final state. The bottom panel displays the muon results divided by the measurements in the electron final state.
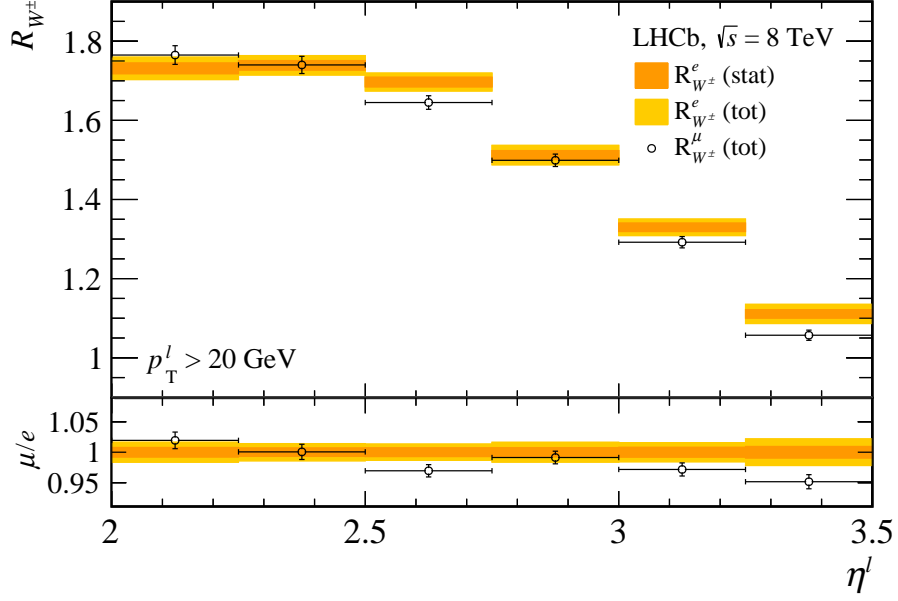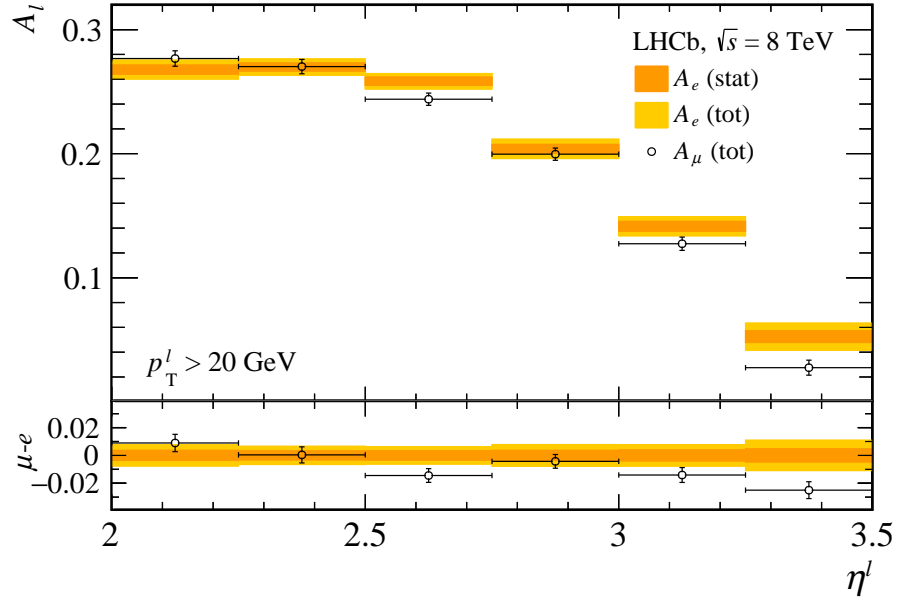

Figure 7: The W boson production charge asymmetry in bins of η^l. The measurement using electrons, represented as bands, is compared to the measurement in the muon final state. The bottom panel displays the difference between the muon and electron final states.
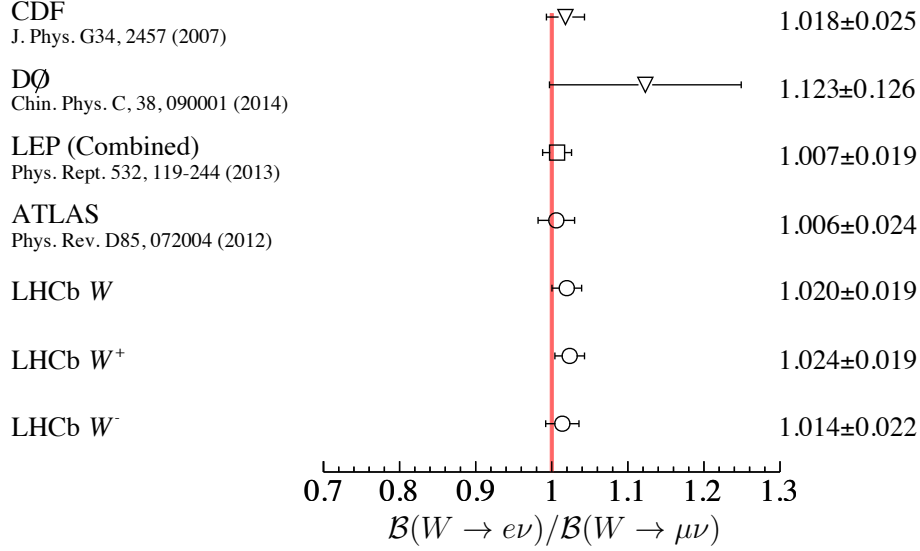
12

Figure 8: The ratio of branching fractions for the electron and muon final states determined for W, W^+, and W^- is compared to hadron collider and LEP results. The theory expectation is represented by the red line.

The consistency with lepton universality is quantified by computing a ratio of W branching fractions using cross-sections determined in the range $2.00 < \eta^l < 3.50$. In this limited acceptance, the ratios of W branching fractions are determined to be

$$
\begin{aligned}
\mathcal{B}(W^+ \to e^+\nu_e)/\mathcal{B}(W^+ \to \mu^+\nu_\mu) &= 1.024 \pm 0.003 \pm 0.019, \\
\mathcal{B}(W^- \to e^-\overline{\nu}_e)/\mathcal{B}(W^- \to \mu^-\overline{\nu}_\mu) &= 1.014 \pm 0.004 \pm 0.022, \\
\mathcal{B}(W \to e\nu)/\mathcal{B}(W \to \mu\nu) \quad\ &= 1.020 \pm 0.002 \pm 0.019,
\end{aligned}
$$

where the first uncertainties are statistical and the second are systematic. The result is compared to past measurements [2, 26, 41, 42] in Fig. 8 and its precision is seen to exceed previous individual determinations of the ratio and to be comparable to the combined LEP result.

8 Conclusions

Measurements of the cross-sections for W boson production in pp collisions are presented at a centre-of-mass energy of $\sqrt{s} = 8\,\mathrm{TeV}$ in the electron final state. The cross-section ratio and the charge asymmetry are also determined. The measurements are found to be in agreement with NNLO calculations in perturbative QCD.

These results represent the first measurements of $W \to e\nu$ production in the forward region at the LHC and are complementary to the previously published measurements of $W \to \mu\nu$ production. The measurements have been performed using statistically independent datasets with largely independent systematic uncertainties. The measurements reported here are found to be consistent with the $W \to \mu\nu$ results.

Comparable precision to the $W \to \mu\nu$ results is achieved in the measurements of the cross-sections and the cross-section ratio has been determined with sub-percent precision. Due to the unique kinematic acceptance of the LHCb detector these results will be valuable in constraining the parton distribution functions of the proton at low and high values of the Bjorken-x variable.

Finally, the measurements of W production in the electron and muon final states are consistent with lepton universality and the ratio of branching fractions has precision that exceeds all past determinations at hadron colliders as well as measurements made at the LEP collider.

Acknowledgements

Appendices

A   Tabulated results

Born level cross-sections in bins of electron pseudorapidity for W^+ (W^-) along with corresponding FSR corrections are given in Table 2 (3). The ratio is given in Table 4 and the charge asymmetry in Table 5.

Table 2: The Born level cross-section for W^+ boson production in bins of electron pseudorapidity. The first uncertainties are statistical, the second are systematic, the third are due to the knowledge of the LHC beam energy and the fourth are due to the luminosity measurement. The rightmost column gives values of the additional factor, f^{FSR}, by which the results should be multiplied in order to give the cross-sections after FSR.

η^e	$\sigma_{W^+ \to e^+ \nu_e}[\,\mathrm{pb}]$	f^{FSR}
2.00 - 2.25	$229.9 \pm 1.0 \pm 6.5 \pm 2.3 \pm 2.7$	0.9671 ± 0.0013
2.25 - 2.50	$210.1 \pm 0.8 \pm 4.7 \pm 2.1 \pm 2.4$	0.9714 ± 0.0013
2.50 - 2.75	$191.7 \pm 0.8 \pm 4.9 \pm 1.9 \pm 2.2$	0.9718 ± 0.0013
2.75 - 3.00	$156.3 \pm 0.7 \pm 3.4 \pm 1.6 \pm 1.8$	0.9741 ± 0.0015
3.00 - 3.25	$132.0 \pm 0.7 \pm 3.1 \pm 1.3 \pm 1.5$	0.9739 ± 0.0016
3.25 - 3.50	$87.6 \pm 0.6 \pm 2.2 \pm 0.9 \pm 1.0$	0.9697 ± 0.0019
3.50 - 3.75	$59.1 \pm 0.5 \pm 2.1 \pm 0.6 \pm 0.7$	0.9727 ± 0.0023
3.75 - 4.25	$57.8 \pm 0.7 \pm 2.7 \pm 0.6 \pm 0.7$	0.9672 ± 0.0024

Table 3: The Born level cross-section for W^- boson production in bins of electron pseudorapidity. The first uncertainties are statistical, the second are systematic, the third are due to the knowledge of the LHC beam energy and the fourth are due to the luminosity measurement. The rightmost column gives values of the additional factor, f^{FSR}, by which the results should be multiplied in order to give the cross-sections after FSR.

η^e	$\sigma_{W^- \to e^- \bar{\nu}_e}[\,\mathrm{pb}]$	f^{FSR}
2.00 - 2.25	$132.8 \pm 0.8 \pm 4.1 \pm 1.1 \pm 1.5$	0.9729 ± 0.0021
2.25 - 2.50	$120.8 \pm 0.7 \pm 3.1 \pm 1.0 \pm 1.4$	0.9726 ± 0.0020
2.50 - 2.75	$113.0 \pm 0.7 \pm 2.9 \pm 1.0 \pm 1.3$	0.9762 ± 0.0020
2.75 - 3.00	$103.3 \pm 0.6 \pm 2.7 \pm 0.9 \pm 1.2$	0.9786 ± 0.0019
3.00 - 3.25	$99.3 \pm 0.6 \pm 2.7 \pm 0.9 \pm 1.2$	0.9746 ± 0.0019
3.25 - 3.50	$78.8 \pm 0.6 \pm 2.2 \pm 0.7 \pm 0.9$	0.9756 ± 0.0019
3.50 - 3.75	$67.0 \pm 0.6 \pm 2.8 \pm 0.6 \pm 0.8$	0.9713 ± 0.0020
3.75 - 4.25	$94.0 \pm 0.9 \pm 4.2 \pm 0.8 \pm 1.1$	0.9653 ± 0.0016

Table 4: The W^+ to W^- cross-section ratio in bins of electron pseudorapidity. The first uncertainties are statistical, the second are systematic and the third are due to the knowledge of the LHC beam energy.

η^e	$R_{W^\pm}$
2.00 - 2.25	$1.731 \pm 0.013 \pm 0.026 \pm 0.003$
2.25 - 2.50	$1.739 \pm 0.012 \pm 0.025 \pm 0.003$
2.50 - 2.75	$1.697 \pm 0.012 \pm 0.022 \pm 0.003$
2.75 - 3.00	$1.512 \pm 0.011 \pm 0.023 \pm 0.002$
3.00 - 3.25	$1.330 \pm 0.011 \pm 0.019 \pm 0.002$
3.25 - 3.50	$1.111 \pm 0.010 \pm 0.025 \pm 0.002$
3.50 - 3.75	$0.882 \pm 0.011 \pm 0.023 \pm 0.001$
3.75 - 4.25	$0.615 \pm 0.010 \pm 0.022 \pm 0.001$

Table 5: The W boson production charge asymmetry in bins of electron pseudorapidity. The first uncertainties are statistical, the second are systematic and the third are due to the knowledge of the LHC beam energy.

η^e	$A_e(\%)$
2.00 - 2.25	$26.78 \pm 0.36 \pm 0.70 \pm 0.07$
2.25 - 2.50	$26.98 \pm 0.32 \pm 0.66 \pm 0.07$
2.50 - 2.75	$25.84 \pm 0.33 \pm 0.60 \pm 0.07$
2.75 - 3.00	$20.39 \pm 0.36 \pm 0.74 \pm 0.07$
3.00 - 3.25	$14.15 \pm 0.39 \pm 0.70 \pm 0.07$
3.25 - 3.50	$5.25 \pm 0.47 \pm 1.11 \pm 0.07$
3.50 - 3.75	$-6.25 \pm 0.60 \pm 1.28 \pm 0.07$
3.75 - 4.25	$-23.85 \pm 0.75 \pm 1.72 \pm 0.07$

B Correlation coefficients

The correlation coefficients of the systematic uncertainties between bins of η^e for the W^+ (W^-) cross-sections are given in Table 6 (7) while those between bins for W^+ and W^- are given in Table 8. The LHC beam energy and luminosity uncertainties, which are fully correlated between cross-section measurements, are excluded.

Table 6: Correlation coefficients of the systematic uncertainties for the differential W^+ cross-section measurement between bins of η^e.

Bin index	1	2	3	4	5	6	7	8
1	1.00							
2	0.93	1.00						
3	0.84	0.80	1.00					
4	0.95	0.94	0.84	1.00				
5	0.95	0.93	0.87	0.99	1.00			
6	0.74	0.79	0.70	0.86	0.85	1.00		
7	0.87	0.86	0.84	0.93	0.94	0.81	1.00	
8	0.82	0.82	0.75	0.88	0.92	0.78	0.86	1.00

Table 7: Correlation coefficients of the systematic uncertainties for the differential W^- cross-section measurement between bins of η^e.

Bin index	1	2	3	4	5	6	7	8
1	1.00							
2	0.99	1.00						
3	0.99	0.99	1.00					
4	0.98	0.99	0.99	1.00				
5	0.98	0.97	0.98	0.99	1.00			
6	0.72	0.75	0.72	0.77	0.76	1.00		
7	0.88	0.89	0.87	0.93	0.93	0.81	1.00	
8	0.84	0.82	0.82	0.87	0.90	0.83	0.95	1.00

Table 8: Correlation coefficients of the systematic uncertainties for the differential W^+ and W^- cross-section measurements between bins of η^e. The horizontal bin indices label bins of η^e for electrons while vertical indices label bins for positrons.

Bin index	1	2	3	4	5	6	7	8
1	0.94	0.95	0.91	0.90	0.86	0.47	0.77	0.67
2	0.87	0.85	0.85	0.81	0.79	0.36	0.65	0.59
3	0.91	0.90	0.93	0.89	0.90	0.56	0.74	0.74
4	0.93	0.92	0.90	0.88	0.87	0.45	0.81	0.71
5	0.95	0.93	0.92	0.90	0.91	0.53	0.85	0.81
6	0.61	0.64	0.65	0.62	0.60	0.67	0.69	0.60
7	0.84	0.82	0.81	0.81	0.83	0.53	0.86	0.82
8	0.84	0.79	0.81	0.79	0.84	0.53	0.81	0.84

C   Fits to lepton p_T

The fits to p_T^e binned in η^e are shown in Figs. 9 and 10. The pulls shown underneath each fit are statistical only. The fractional signal contribution in the W^+ (W^-) sample varies from ~70%(~60%) near $\eta^e = 2$ to ~40%(~50%) at the largest pseudorapidity. The values of χ^2/ndf for the fits range between 0.9 and 2.3, based on statistical uncertainties only. The systematic uncertainties in the event yields presented in Section 6 are found to cover the uncertainty that arises from imperfect fit quality.
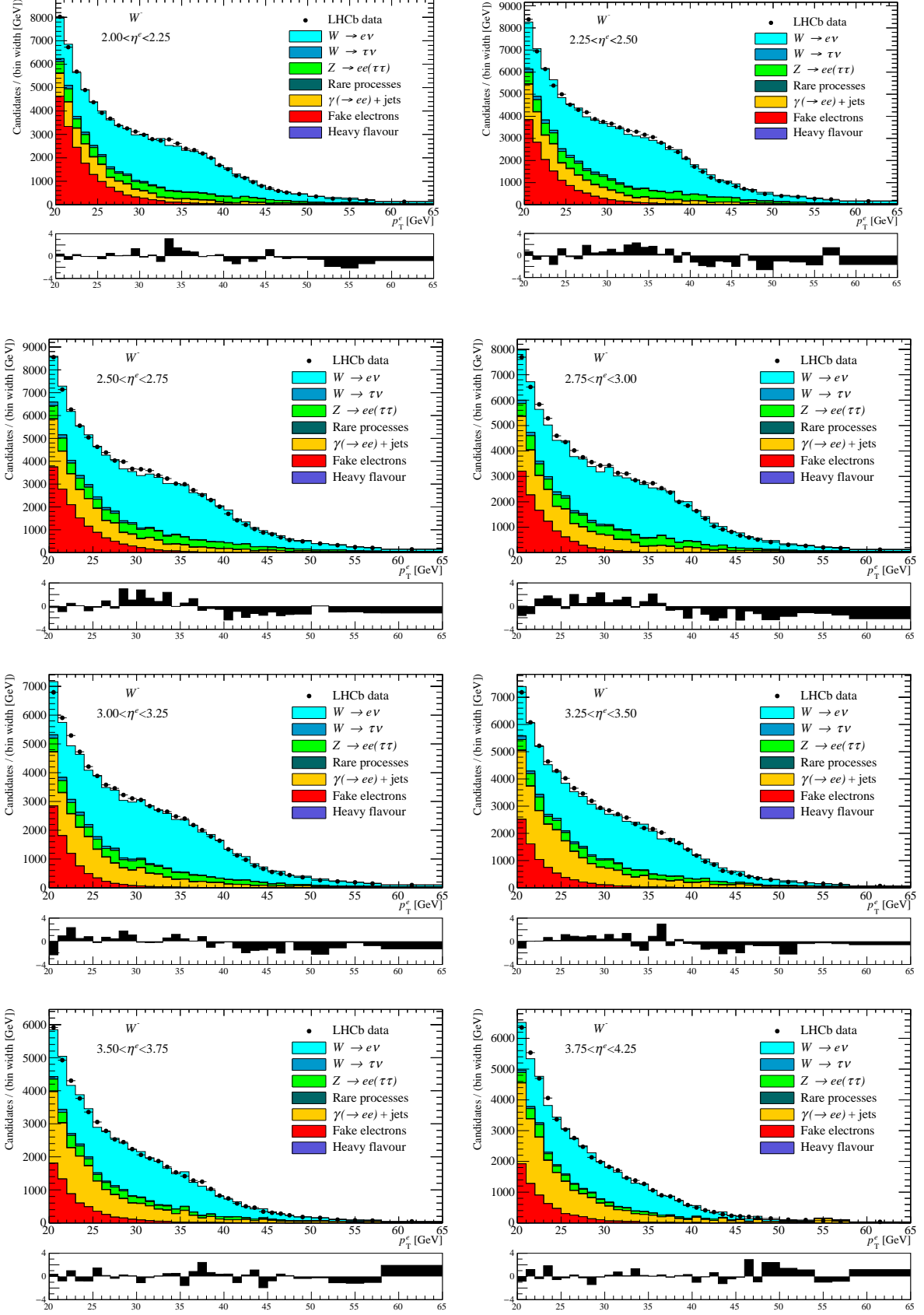
Figure 9: Fits to p_{T}^e for e^- in bins of η^e. Pulls are shown underneath.
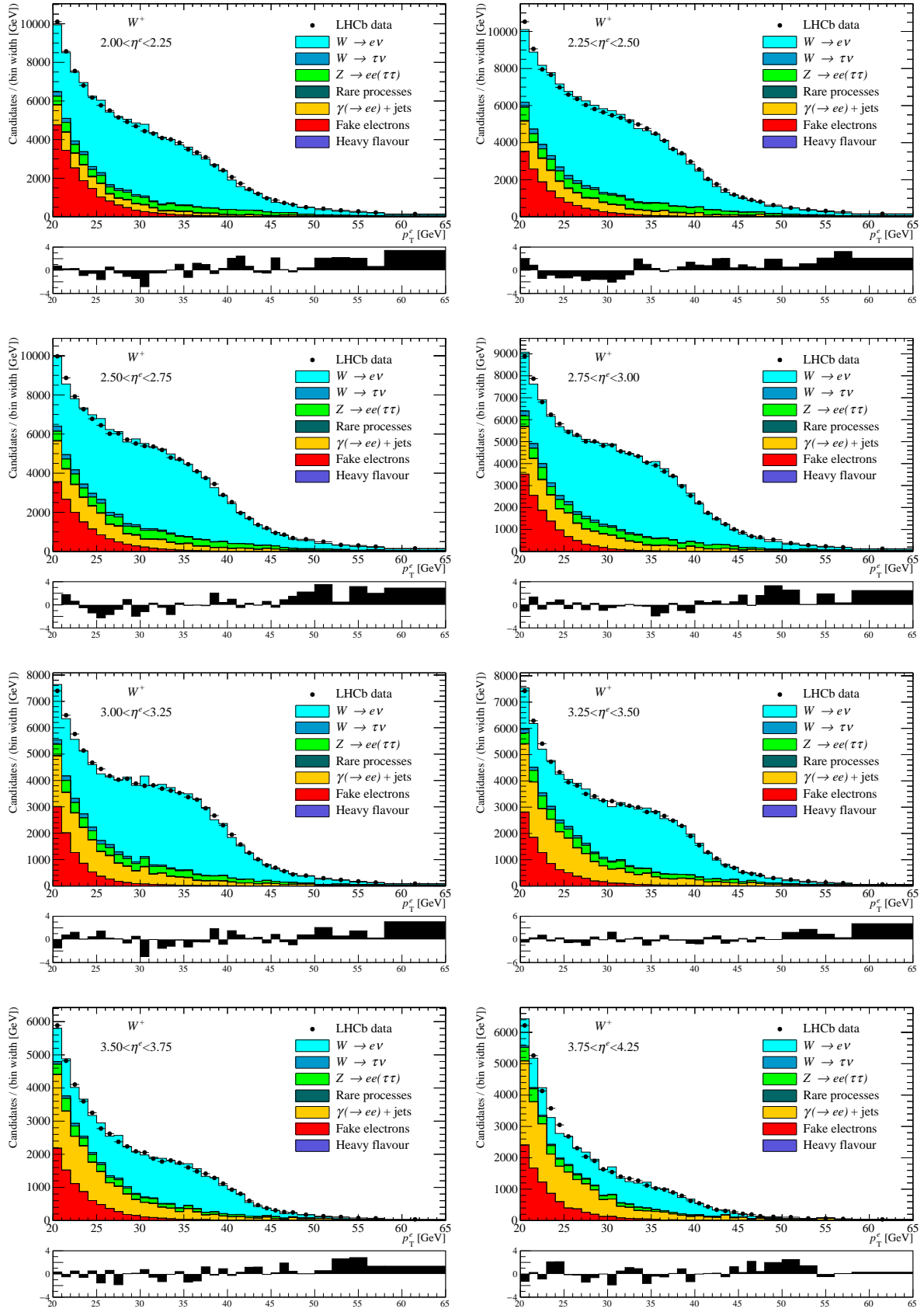
Figure 10: Fits to p_T^e for e^+ in bins of η^e. Pulls are shown underneath.

References

[1] J. Butterworth *et al.*, *PDF4LHC recommendations for LHC Run II*, J. Phys. **G43** (2016) 023001, `arXiv:1510.03865`.

[2] ATLAS collaboration, G. Aad *et al.*, *Measurement of the inclusive $W^{\pm}$ and Z/γ^* cross sections in the electron and muon decay channels in pp collisions at $\sqrt{s} = 7$ TeV with the ATLAS detector*, Phys. Rev. **D85** (2012) 072004, `arXiv:1109.5141`.

[3] ATLAS collaboration, G. Aad *et al.*, *Measurement of the double-differential high-mass Drell–Yan cross section in pp collisions at $\sqrt{s} = 8$ TeV with the ATLAS detector*, JHEP **08** (2016) 009, `arXiv:1606.01736`.

[4] ATLAS collaboration, G. Aad *et al.*, *Measurement of $W^{\pm}$ and Z-boson production cross sections in pp collisions at $\sqrt{s} = 13$ TeV with the ATLAS detector*, Phys. Lett. **B759** (2016) 601, `arXiv:1603.09222`.

[5] CMS collaboration, V. Khachatryan *et al.*, *Measurement of the transverse momentum spectra of weak vector bosons produced in proton–proton collisions at $\sqrt{s} = 8$ TeV*, `arXiv:1606.05864`, submitted to JHEP.

[6] CMS collaboration, V. Khachatryan *et al.*, *Measurement of the differential cross section and charge asymmetry for inclusive $pp \to W + X$ production at $\sqrt{s} = 8$ TeV*, Eur. Phys. J. **C76** (2016), no. 8 469, `arXiv:1603.01803`.

[7] CMS collaboration, S. Chatrchyan *et al.*, *Measurement of inclusive W and Z boson production cross sections in pp collisions at $\sqrt{s} = 8$ TeV*, Phys. Rev. Lett. **112** (2014) 191802, `arXiv:1402.0923`.

[8] LHCb collaboration, R. Aaij *et al.*, *Measurement of the forward W boson production cross-section in pp collisions at $\sqrt{s} = 7$ TeV*, JHEP **12** (2014) 079, `arXiv:1408.4354`.

[9] LHCb collaboration, R. Aaij *et al.*, *Measurement of forward W and Z boson production in pp collisions at $\sqrt{s} = 8$ TeV*, JHEP **01** (2016) 155, `arXiv:1511.08039`.

[10] LHCb collaboration, R. Aaij *et al.*, *Measurement of the forward Z boson production cross-section in pp collisions at $\sqrt{s} = 7$ TeV*, JHEP **08** (2015) 039, `arXiv:1505.07024`.

[11] LHCb collaboration, R. Aaij *et al.*, *Measurement of the cross-section for $Z \to e^+e^-$ production in pp collisions at $\sqrt{s} = 7$ TeV*, JHEP **02** (2013) 106, `arXiv:1212.4620`.

[12] LHCb collaboration, R. Aaij *et al.*, *Measurement of forward $Z \to e^+e^-$ production in pp collisions at $\sqrt{s} = 8$ TeV*, JHEP **05** (2015) 109, `arXiv:1503.00963`.

[13] LHCb collaboration, R. Aaij *et al.*, *A study of the Z production cross-section in pp collisions at $\sqrt{s} = 7$ TeV using tau final states*, JHEP **01** (2013) 111, `arXiv:1210.6289`.

[14] LHCb collaboration, R. Aaij *et al.*, *Measurement of the forward Z boson production cross-section in pp collisions at $\sqrt{s} = 13$ TeV*, JHEP **09** (2016) 136, `arXiv:1607.06495`.

[15] R. Gavin, Y. Li, F. Petriello, and S. Quackenbush, *FEWZ 2.0: A code for hadronic Z production at next-to-next-to-leading order*, Comput. Phys. Commun. **182** (2011) 2388, `arXiv:1011.3540`.

[16] Y. Li and F. Petriello, *Combining QCD and electroweak corrections to dilepton production in FEWZ*, Phys. Rev. **D86** (2012) 094034, `arXiv:1208.5967`.

[17] LHCb collaboration, A. A. Alves Jr. *et al.*, *The LHCb detector at the LHC*, JINST **3** (2008) S08005.

[18] LHCb collaboration, R. Aaij *et al*, *LHCb detector performance*, Int. J. Mod. Phys. **A30** (2015) 1530022, `arXiv:1412.6352`.

[19] T. Sjöstrand, S. Mrenna, and P. Skands, *A brief introduction to PYTHIA 8.1*, Comput. Phys. Commun. **178** (2008) 852, `arXiv:0710.3820`; T. Sjöstrand, S. Mrenna, and P. Skands, *PYTHIA 6.4 physics and manual*, JHEP **05** (2006) 026, `arXiv:hep-ph/0603175`.

[20] I. Belyaev *et al.*, *Handling of the generation of primary events in Gauss, the LHCb simulation framework*, J. Phys. Conf. Ser. **331** (2011) 032047.

[21] Geant4 collaboration, J. Allison *et al.*, *Geant4 developments and applications*, IEEE Trans. Nucl. Sci. **53** (2006) 270; Geant4 collaboration, S. Agostinelli *et al.*, *Geant4: A simulation toolkit*, Nucl. Instrum. Meth. **A506** (2003) 250.

[22] M. Clemencic *et al.*, *The LHCb simulation application, Gauss: Design, evolution and experience*, J. Phys. Conf. Ser. **331** (2011) 032023.

[23] P. M. Nadolsky *et al.*, *Implications of CTEQ global analysis for collider observables*, Phys. Rev. **D78** (2008) 013004, `arXiv:0802.0007`.

[24] T. Sjöstrand and P. Z. Skands, *Transverse-momentum-ordered showers and interleaved multiple interactions*, Eur. Phys. J. **C39** (2005) 129, `arXiv:hep-ph/0408302`.

[25] R. J. Barlow and C. Beeston, *Fitting using finite Monte Carlo samples*, Comput. Phys. Commun. **77** (1993) 219.

[26] Particle Data Group, K. A. Olive *et al.*, *Review of particle physics*, Chin. Phys. **C38** (2014) 090001, and 2015 update.

[27] J. M. Campbell and R. K. Ellis, *MCFM for the Tevatron and the LHC*, Nucl. Phys. Proc. Suppl. **205-206** (2010) 10, `arXiv:1007.3492`.

[28] G. A. Ladinsky and C. P. Yuan, *The Nonperturbative regime in QCD resummation for gauge boson production at hadron colliders*, Phys. Rev. **D50** (1994) 4239, `arXiv:hep-ph/9311341`.

[29] C. Balazs and C. P. Yuan, *Soft gluon effects on lepton pairs at hadron colliders*, Phys. Rev. **D56** (1997) 5558, `arXiv:hep-ph/9704258`.

[30] F. Landry, R. Brock, P. M. Nadolsky, and C. P. Yuan, *Tevatron Run-1 Z boson data and Collins-Soper-Sterman resummation formalism*, Phys. Rev. **D67** (2003) 073016, `arXiv:hep-ph/0212159`.

[31] M. Bahr *et al.*, *Herwig++ physics and manual*, Eur. Phys. J. **C58** (2008) 639, `arXiv:0803.0883`.

[32] J. Wenninger, *Energy calibration of the LHC beams at 4 TeV*, Tech. Rep. CERN-ATS-2013-040, CERN, Geneva.

[33] S. Catani *et al.*, *Vector boson production at hadron colliders: A fully exclusive QCD calculation at NNLO*, Phys. Rev. Lett. **103** (2009) 082001, `arXiv:0903.2120`.

[34] LHCb collaboration, R. Aaij *et al.*, *Precision luminosity measurements at LHCb*, JINST **9** (2014) P12005, `arXiv:1410.0149`.

[35] S. Alekhin, J. Blümlein, and S. Moch, *The ABM parton distributions tuned to LHC data*, Phys. Rev. **D89** (2014) 054028, `arXiv:1310.3059`.

[36] S. Dulat *et al.*, *New parton distribution functions from a global analysis of quantum chromodynamics*, Phys. Rev. **D93** (2016) 033006, `arXiv:1506.07443`.

[37] ZEUS, H1 collaborations, A. M. Cooper-Sarkar, *PDF Fits at HERA*, PoS **EPS-HEP2011** (2011) 320, `arXiv:1112.2107`.

[38] L. A. Harland-Lang, A. D. Martin, P. Motylinski, and R. S. Thorne, *Parton distributions in the LHC era: MMHT 2014 PDFs*, Eur. Phys. J. **C75** (2015) 204, `arXiv:1412.3989`.

[39] A. D. Martin, W. J. Stirling, R. S. Thorne, and G. Watt, *Parton distributions for the LHC*, Eur. Phys. J. **C63** (2009) 189, `arXiv:0901.0002`.

[40] NNPDF collaboration, R. D. Ball *et al.*, *Parton distributions for the LHC Run II*, JHEP **04** (2015) 040, `arXiv:1410.8849`.

[41] CDF collaboration, A. Abulencia *et al.*, *Measurements of inclusive W and Z cross sections in $p\bar{p}$ collisions at $\sqrt{s}$ = 1.96 TeV*, J. Phys. **G34** (2007) 2457, `arXiv:hep-ex/0508029`.

[42] ALEPH, DELPHI, L3, OPAL collaborations, LEP Electroweak working group, S. Schael *et al.*, *Electroweak measurements in electron-positron collisions at W-boson-pair energies at LEP*, Phys. Rept. **532** (2013) 119, `arXiv:1302.3415`.

LHCb collaboration

R. Aaij[40], B. Adeva[39], M. Adinolfi[48], Z. Ajaltouni[5], S. Akar[6], J. Albrecht[10], F. Alessio[40],
M. Alexander[53], S. Ali[43], G. Alkhazov[31], P. Alvarez Cartelle[55], A.A. Alves Jr[59], S. Amato[2],
S. Amerio[23], Y. Amhis[7], L. An[41], L. Anderlini[18], G. Andreassi[41], M. Andreotti[17,g],
J.E. Andrews[60], R.B. Appleby[56], O. Aquines Gutierrez[11], F. Archilli[43], P. d'Argent[12],
J. Arnau Romeu[6], A. Artamonov[37], M. Artuso[61], E. Aslanides[6], G. Auriemma[26], M. Baalouch[5],
I. Babuschkin[56], S. Bachmann[12], J.J. Back[50], A. Badalov[38], C. Baesso[62], W. Baldini[17],
R.J. Barlow[56], C. Barschel[40], S. Barsuk[7], W. Barter[40], V. Batozskaya[29], B. Batsukh[61],
V. Battista[41], A. Bay[41], L. Beaucourt[4], J. Beddow[53], F. Bedeschi[24], I. Bediaga[1], L.J. Bel[43],
V. Bellee[41], N. Belloli[21,i], K. Belous[37], I. Belyaev[32], E. Ben-Haim[8], G. Bencivenni[19],
S. Benson[40], J. Benton[48], A. Berezhnoy[33], R. Bernet[42], A. Bertolin[23], F. Betti[15],
M.-O. Bettler[40], M. van Beuzekom[43], I. Bezshyiko[42], S. Bifani[47], P. Billoir[8], T. Bird[56],
A. Birnkraut[10], A. Bitadze[56], A. Bizzeti[18,u], T. Blake[50], F. Blanc[41], J. Blouw[11], S. Blusk[61],
V. Bocci[26], T. Boettcher[58], A. Bondar[36], N. Bondar[31,40], W. Bonivento[16], A. Borgheresi[21,i],
S. Borghi[56], M. Borisyak[35], M. Borsato[39], F. Bossu[7], M. Boubdir[9], T.J.V. Bowcock[54],
E. Bowen[42], C. Bozzi[17,40], S. Braun[12], M. Britsch[12], T. Britton[61], J. Brodzicka[56],
E. Buchanan[48], C. Burr[56], A. Bursche[2], J. Buytaert[40], S. Cadeddu[16], R. Calabrese[17,g],
M. Calvi[21,i], M. Calvo Gomez[38,m], A. Camboni[38], P. Campana[19], D. Campora Perez[40],
D.H. Campora Perez[40], L. Capriotti[56], A. Carbone[15,e], G. Carboni[25,j], R. Cardinale[20,h],
A. Cardini[16], P. Carniti[21,i], L. Carson[52], K. Carvalho Akiba[2], G. Casse[54], L. Cassina[21,i],
L. Castillo Garcia[41], M. Cattaneo[40], Ch. Cauet[10], G. Cavallero[20], R. Cenci[24,t], M. Charles[8],
Ph. Charpentier[40], G. Chatzikonstantinidis[47], M. Chefdeville[4], S. Chen[56], S.-F. Cheung[57],
V. Chobanova[39], M. Chrzaszcz[42,27], X. Cid Vidal[39], G. Ciezarek[43], P.E.L. Clarke[52],
M. Clemencic[40], H.V. Cliff[49], J. Closier[40], V. Coco[59], J. Cogan[6], E. Cogneras[5], V. Cogoni[16,40,f],
L. Cojocariu[30], G. Collazuol[23,o], P. Collins[40], A. Comerma-Montells[12], A. Contu[40], A. Cook[48],
S. Coquereau[8], G. Corti[40], M. Corvo[17,g], C.M. Costa Sobral[50], B. Couturier[40], G.A. Cowan[52],
D.C. Craik[52], A. Crocombe[50], M. Cruz Torres[62], S. Cunliffe[55], R. Currie[55], C. D'Ambrosio[40],
E. Dall'Occo[43], J. Dalseno[48], P.N.Y. David[43], A. Davis[59], O. De Aguiar Francisco[2],
K. De Bruyn[6], S. De Capua[56], M. De Cian[12], J.M. De Miranda[1], L. De Paula[2], M. De Serio[14,d],
P. De Simone[19], C.-T. Dean[53], D. Decamp[4], M. Deckenhoff[10], L. Del Buono[8], M. Demmer[10],
D. Derkach[35], O. Deschamps[5], F. Dettori[40], B. Dey[22], A. Di Canto[40], H. Dijkstra[40],
F. Dordei[40], M. Dorigo[41], A. Dosil Suárez[39], A. Dovbnya[45], K. Dreimanis[54], L. Dufour[43],
G. Dujany[56], K. Dungs[40], P. Durante[40], R. Dzhelyadin[37], A. Dziurda[40], A. Dzyuba[31],
N. Déléage[4], S. Easo[51], M. Ebert[52], U. Egede[55], V. Egorychev[32], S. Eidelman[36], S. Eisenhardt[52],
U. Eitschberger[10], R. Ekelhof[10], L. Eklund[53], Ch. Elsasser[42], S. Ely[61], S. Esen[12], H.M. Evans[49],
T. Evans[57], A. Falabella[15], N. Farley[47], S. Farry[54], R. Fay[54], D. Fazzini[21,i], D. Ferguson[52],
V. Fernandez Albor[39], A. Fernandez Prieto[39], F. Ferrari[15,40], F. Ferreira Rodrigues[1],
M. Ferro-Luzzi[40], S. Filippov[34], R.A. Fini[14], M. Fiore[17,g], M. Fiorini[17,g], M. Firlej[28],
C. Fitzpatrick[41], T. Fiutowski[28], F. Fleuret[7,b], K. Fohl[40], M. Fontana[16], F. Fontanelli[20,h],
D.C. Forshaw[61], R. Forty[40], V. Franco Lima[54], M. Frank[40], C. Frei[40], J. Fu[22,q], E. Furfaro[25,j],
C. Färber[40], A. Gallas Torreira[39], D. Galli[15,e], S. Gallorini[23], S. Gambetta[52], M. Gandelman[2],
P. Gandini[57], Y. Gao[3], L.M. Garcia Martin[68], J. García Pardiñas[39], J. Garra Tico[49],
L. Garrido[38], P.J. Garsed[49], D. Gascon[38], C. Gaspar[40], L. Gavardi[10], G. Gazzoni[5], D. Gerick[12],
E. Gersabeck[12], M. Gersabeck[56], T. Gershon[50], Ph. Ghez[4], S. Gianì[41], V. Gibson[49],
O.G. Girard[41], L. Giubega[30], K. Gizdov[52], V.V. Gligorov[8], D. Golubkov[32], A. Golutvin[55,40],
A. Gomes[1,a], I.V. Gorelov[33], C. Gotti[21,i], M. Grabalosa Gándara[5], R. Graciani Diaz[38],
L.A. Granado Cardoso[40], E. Graugés[38], E. Graverini[42], G. Graziani[18], A. Grecu[30], P. Griffith[47],
L. Grillo[21], B.R. Gruberg Cazon[57], O. Grünberg[66], E. Gushchin[34], Yu. Guz[37], T. Gys[40],
C. Göbel[62], T. Hadavizadeh[57], C. Hadjivasiliou[5], G. Haefeli[41], C. Haen[40], S.C. Haines[49],

S. Hall[55], B. Hamilton[60], X. Han[12], S. Hansmann-Menzemer[12], N. Harnew[57], S.T. Harnew[48], J. Harrison[56], M. Hatch[40], J. He[63], T. Head[41], A. Heister[9], K. Hennessy[54], P. Henrard[5], L. Henry[8], J.A. Hernando Morata[39], E. van Herwijnen[40], M. Heß[66], A. Hicheur[2], D. Hill[57], C. Hombach[56], H. Hopchev[41], W. Hulsbergen[43], T. Humair[55], M. Hushchyn[35], N. Hussain[57], D. Hutchcroft[54], V. Iakovenko[46], M. Idzik[28], P. Ilten[58], R. Jacobsson[40], A. Jaeger[12], J. Jalocha[57], E. Jans[43], A. Jawahery[60], M. John[57], D. Johnson[40], C.R. Jones[49], C. Joram[40], B. Jost[40], N. Jurik[61], S. Kandybei[45], W. Kanso[6], M. Karacson[40], J.M. Kariuki[48], S. Karodia[53], M. Kecke[12], M. Kelsey[61], I.R. Kenyon[47], M. Kenzie[40], T. Ketel[44], E. Khairullin[35], B. Khanji[21,40,i], C. Khurewathanakul[41], T. Kirn[9], S. Klaver[56], K. Klimaszewski[29], S. Koliiev[46], M. Kolpin[12], I. Komarov[41], R.F. Koopman[44], P. Koppenburg[43], A. Kozachuk[33], M. Kozeiha[5], L. Kravchuk[34], K. Kreplin[12], M. Kreps[50], P. Krokovny[36], F. Kruse[10], W. Krzemien[29], W. Kucewicz[27,l], M. Kucharczyk[27], V. Kudryavtsev[36], A.K. Kuonen[41], K. Kurek[29], T. Kvaratskheliya[32,40], D. Lacarrere[40], G. Lafferty[56,40], A. Lai[16], D. Lambert[52], G. Lanfranchi[19], C. Langenbruch[9], B. Langhans[40], T. Latham[50], C. Lazzeroni[47], R. Le Gac[6], J. van Leerdam[43], J.-P. Lees[4], A. Leflat[33,40], J. Lefrançois[7], R. Lefèvre[5], F. Lemaitre[40], E. Lemos Cid[39], O. Leroy[6], T. Lesiak[27], B. Leverington[12], Y. Li[7], T. Likhomanenko[35,67], R. Lindner[40], C. Linn[40], F. Lionetto[42], B. Liu[16], X. Liu[3], D. Loh[50], I. Longstaff[53], J.H. Lopes[2], D. Lucchesi[23,o], M. Lucio Martinez[39], H. Luo[52], A. Lupato[23], E. Luppi[17,g], O. Lupton[57], A. Lusiani[24], X. Lyu[63], F. Machefert[7], F. Maciuc[30], O. Maev[31], K. Maguire[56], S. Malde[57], A. Malinin[67], T. Maltsev[36], G. Manca[7], G. Mancinelli[6], P. Manning[61], J. Maratas[5,v], J.F. Marchand[4], U. Marconi[15], C. Marin Benito[38], P. Marino[24,t], J. Marks[12], G. Martellotti[26], M. Martin[6], M. Martinelli[41], D. Martinez Santos[39], F. Martinez Vidal[68], D. Martins Tostes[2], L.M. Massacrier[7], A. Massafferri[1], R. Matev[40], A. Mathad[50], Z. Mathe[40], C. Matteuzzi[21], A. Mauri[42], B. Maurin[41], A. Mazurov[47], M. McCann[55], J. McCarthy[47], A. McNab[56], R. McNulty[13], B. Meadows[59], F. Meier[10], M. Meissner[12], D. Melnychuk[29], M. Merk[43], A. Merli[22,q], E. Michielin[23], D.A. Milanes[65], M.-N. Minard[4], D.S. Mitzel[12], A. Mogini[8], J. Molina Rodriguez[62], I.A. Monroy[65], S. Monteil[5], M. Morandin[23], P. Morawski[28], A. Mordà[6], M.J. Morello[24,t], J. Moron[28], A.B. Morris[52], R. Mountain[61], F. Muheim[52], M. Mulder[43], M. Mussini[15], D. Müller[56], J. Müller[10], K. Müller[42], V. Müller[10], P. Naik[48], T. Nakada[41], R. Nandakumar[51], A. Nandi[57], I. Nasteva[2], M. Needham[52], N. Neri[22], S. Neubert[12], N. Neufeld[40], M. Neuner[12], A.D. Nguyen[41], C. Nguyen-Mau[41,n], S. Nieswand[9], R. Niet[10], N. Nikitin[33], T. Nikodem[12], A. Novoselov[37], D.P. O'Hanlon[50], A. Oblakowska-Mucha[28], V. Obraztsov[37], S. Ogilvy[19], R. Oldeman[49], C.J.G. Onderwater[69], J.M. Otalora Goicochea[2], A. Otto[40], P. Owen[42], A. Oyanguren[68], P.R. Pais[41], A. Palano[14,d], F. Palombo[22,q], M. Palutan[19], J. Panman[40], A. Papanestis[51], M. Pappagallo[14,d], L.L. Pappalardo[17,g], W. Parker[60], C. Parkes[56], G. Passaleva[18], A. Pastore[14,d], G.D. Patel[54], M. Patel[55], C. Patrignani[15,e], A. Pearce[56,51], A. Pellegrino[43], G. Penso[26,k], M. Pepe Altarelli[40], S. Perazzini[40], P. Perret[5], L. Pescatore[47], K. Petridis[48], A. Petrolini[20,h], A. Petrov[67], M. Petruzzo[22,q], E. Picatoste Olloqui[38], B. Pietrzyk[4], M. Pikies[27], D. Pinci[26], A. Pistone[20], A. Piucci[12], S. Playfer[52], M. Plo Casasus[39], T. Poikela[40], F. Polci[8], A. Poluektov[50,36], I. Polyakov[61], E. Polycarpo[2], G.J. Pomery[48], A. Popov[37], D. Popov[11,40], B. Popovici[30], S. Poslavskii[37], C. Potterat[2], E. Price[48], J.D. Price[54], J. Prisciandaro[39], A. Pritchard[54], C. Prouve[48], V. Pugatch[46], A. Puig Navarro[41], G. Punzi[24,p], W. Qian[57], R. Quagliani[7,48], B. Rachwal[27], J.H. Rademacker[48], M. Rama[24], M. Ramos Pernas[39], M.S. Rangel[2], I. Raniuk[45], G. Raven[44], F. Redi[55], S. Reichert[10], A.C. dos Reis[1], C. Remon Alepuz[68], V. Renaudin[7], S. Ricciardi[51], S. Richards[48], M. Rihl[40], K. Rinnert[54,40], V. Rives Molina[38], P. Robbe[7,40], A.B. Rodrigues[1], E. Rodrigues[59], J.A. Rodriguez Lopez[65], P. Rodriguez Perez[56], A. Rogozhnikov[35], S. Roiser[40], V. Romanovskiy[37], A. Romero Vidal[39], J.W. Ronayne[13], M. Rotondo[19], M.S. Rudolph[61], T. Ruf[40], P. Ruiz Valls[68], J.J. Saborido Silva[39], E. Sadykhov[32], N. Sagidova[31], B. Saitta[16,f], V. Salustino Guimaraes[2], C. Sanchez Mayordomo[68], B. Sanmartin Sedes[39], R. Santacesaria[26],

25

C. Santamarina Rios[39], M. Santimaria[19], E. Santovetti[25,j], A. Sarti[19,k], C. Satriano[26,s],
A. Satta[25], D.M. Saunders[48], D. Savrina[32,33], S. Schael[9], M. Schellenberg[10], M. Schiller[40],
H. Schindler[40], M. Schlupp[10], M. Schmelling[11], T. Schmelzer[10], B. Schmidt[40], O. Schneider[41],
A. Schopper[40], K. Schubert[10], M. Schubiger[41], M.-H. Schune[7], R. Schwemmer[40], B. Sciascia[19],
A. Sciubba[26,k], A. Semennikov[32], A. Sergi[47], N. Serra[42], J. Serrano[6], L. Sestini[23], P. Seyfert[21],
M. Shapkin[37], I. Shapoval[17,45,g], Y. Shcheglov[31], T. Shears[54], L. Shekhtman[36], V. Shevchenko[67],
A. Shires[10], B.G. Siddi[17], R. Silva Coutinho[42], L. Silva de Oliveira[2], G. Simi[23,o], S. Simone[14,d],
M. Sirendi[49], N. Skidmore[48], T. Skwarnicki[61], E. Smith[55], I.T. Smith[52], J. Smith[49], M. Smith[55],
H. Snoek[43], M.D. Sokoloff[59], F.J.P. Soler[53], D. Souza[48], B. Souza De Paula[2], B. Spaan[10],
P. Spradlin[53], S. Sridharan[40], F. Stagni[40], M. Stahl[12], S. Stahl[40], P. Stefko[41], S. Stefkova[55],
O. Steinkamp[42], S. Stemmle[12], O. Stenyakin[37], S. Stevenson[57], S. Stoica[30], S. Stone[61],
B. Storaci[42], S. Stracka[24,t], M. Straticiuc[30], U. Straumann[42], L. Sun[59], W. Sutcliffe[55],
K. Swientek[28], V. Syropoulos[44], M. Szczekowski[29], T. Szumlak[28], S. T'Jampens[4],
A. Tayduganov[6], T. Tekampe[10], G. Tellarini[17,g], F. Teubert[40], C. Thomas[57], E. Thomas[40],
J. van Tilburg[43], V. Tisserand[4], M. Tobin[41], S. Tolk[49], L. Tomassetti[17,g], D. Tonelli[40],
S. Topp-Joergensen[57], F. Toriello[61], E. Tournefier[4], S. Tourneur[41], K. Trabelsi[41], M. Traill[53],
M.T. Tran[41], M. Tresch[42], A. Trisovic[40], A. Tsaregorodtsev[6], P. Tsopelas[43], A. Tully[49],
N. Tuning[43], A. Ukleja[29], A. Ustyuzhanin[35,67], U. Uwer[12], C. Vacca[16,40,f], V. Vagnoni[15,40],
S. Valat[40], G. Valenti[15], A. Vallier[7], R. Vazquez Gomez[19], P. Vazquez Regueiro[39], S. Vecchi[17],
M. van Veghel[43], J.J. Velthuis[48], M. Veltri[18,r], G. Veneziano[41], A. Venkateswaran[61], M. Vernet[5],
M. Vesterinen[12], B. Viaud[7], D. Vieira[1], M. Vieites Diaz[39], X. Vilasis-Cardona[38,m], V. Volkov[33],
A. Vollhardt[42], B. Voneki[40], D. Voong[48], A. Vorobyev[31], V. Vorobyev[36], C. Voß[66],
J.A. de Vries[43], C. Vázquez Sierra[39], R. Waldi[66], C. Wallace[50], R. Wallace[13], J. Walsh[24],
J. Wang[61], D.R. Ward[49], H.M. Wark[54], N.K. Watson[47], D. Websdale[55], A. Weiden[42],
M. Whitehead[40], J. Wicht[50], G. Wilkinson[57,40], M. Wilkinson[61], M. Williams[40],
M.P. Williams[47], M. Williams[58], T. Williams[47], F.F. Wilson[51], J. Wimberley[60], J. Wishahi[10],
W. Wislicki[29], M. Witek[27], G. Wormser[7], S.A. Wotton[49], K. Wraight[53], S. Wright[49],
K. Wyllie[40], Y. Xie[64], Z. Xing[61], Z. Xu[41], Z. Yang[3], H. Yin[64], J. Yu[64], X. Yuan[36],
O. Yushchenko[37], M. Zangoli[15], K.A. Zarebski[47], M. Zavertyaev[11,c], L. Zhang[3], Y. Zhang[7],
Y. Zhang[63], A. Zhelezov[12], Y. Zheng[63], A. Zhokhov[32], X. Zhu[3], V. Zhukov[9], S. Zucchelli[15].

[1]*Centro Brasileiro de Pesquisas Físicas (CBPF), Rio de Janeiro, Brazil*
[2]*Universidade Federal do Rio de Janeiro (UFRJ), Rio de Janeiro, Brazil*
[3]*Center for High Energy Physics, Tsinghua University, Beijing, China*
[4]*LAPP, Université Savoie Mont-Blanc, CNRS/IN2P3, Annecy-Le-Vieux, France*
[5]*Clermont Université, Université Blaise Pascal, CNRS/IN2P3, LPC, Clermont-Ferrand, France*
[6]*CPPM, Aix-Marseille Université, CNRS/IN2P3, Marseille, France*
[7]*LAL, Université Paris-Sud, CNRS/IN2P3, Orsay, France*
[8]*LPNHE, Université Pierre et Marie Curie, Université Paris Diderot, CNRS/IN2P3, Paris, France*
[9]*I. Physikalisches Institut, RWTH Aachen University, Aachen, Germany*
[10]*Fakultät Physik, Technische Universität Dortmund, Dortmund, Germany*
[11]*Max-Planck-Institut für Kernphysik (MPIK), Heidelberg, Germany*
[12]*Physikalisches Institut, Ruprecht-Karls-Universität Heidelberg, Heidelberg, Germany*
[13]*School of Physics, University College Dublin, Dublin, Ireland*
[14]*Sezione INFN di Bari, Bari, Italy*
[15]*Sezione INFN di Bologna, Bologna, Italy*
[16]*Sezione INFN di Cagliari, Cagliari, Italy*
[17]*Sezione INFN di Ferrara, Ferrara, Italy*
[18]*Sezione INFN di Firenze, Firenze, Italy*
[19]*Laboratori Nazionali dell'INFN di Frascati, Frascati, Italy*
[20]*Sezione INFN di Genova, Genova, Italy*
[21]*Sezione INFN di Milano Bicocca, Milano, Italy*
[22]*Sezione INFN di Milano, Milano, Italy*

[23]Sezione INFN di Padova, Padova, Italy

[24]Sezione INFN di Pisa, Pisa, Italy

[25]Sezione INFN di Roma Tor Vergata, Roma, Italy

[26]Sezione INFN di Roma La Sapienza, Roma, Italy

[27]Henryk Niewodniczanski Institute of Nuclear Physics Polish Academy of Sciences, Kraków, Poland

[28]AGH - University of Science and Technology, Faculty of Physics and Applied Computer Science, Kraków, Poland

[29]National Center for Nuclear Research (NCBJ), Warsaw, Poland

[30]Horia Hulubei National Institute of Physics and Nuclear Engineering, Bucharest-Magurele, Romania

[31]Petersburg Nuclear Physics Institute (PNPI), Gatchina, Russia

[32]Institute of Theoretical and Experimental Physics (ITEP), Moscow, Russia

[33]Institute of Nuclear Physics, Moscow State University (SINP MSU), Moscow, Russia

[34]Institute for Nuclear Research of the Russian Academy of Sciences (INR RAN), Moscow, Russia

[35]Yandex School of Data Analysis, Moscow, Russia

[36]Budker Institute of Nuclear Physics (SB RAS) and Novosibirsk State University, Novosibirsk, Russia

[37]Institute for High Energy Physics (IHEP), Protvino, Russia

[38]ICCUB, Universitat de Barcelona, Barcelona, Spain

[39]Universidad de Santiago de Compostela, Santiago de Compostela, Spain

[40]European Organization for Nuclear Research (CERN), Geneva, Switzerland

[41]Ecole Polytechnique Fédérale de Lausanne (EPFL), Lausanne, Switzerland

[42]Physik-Institut, Universität Zürich, Zürich, Switzerland

[43]Nikhef National Institute for Subatomic Physics, Amsterdam, The Netherlands

[44]Nikhef National Institute for Subatomic Physics and VU University Amsterdam, Amsterdam, The Netherlands

[45]NSC Kharkiv Institute of Physics and Technology (NSC KIPT), Kharkiv, Ukraine

[46]Institute for Nuclear Research of the National Academy of Sciences (KINR), Kyiv, Ukraine

[47]University of Birmingham, Birmingham, United Kingdom

[48]H.H. Wills Physics Laboratory, University of Bristol, Bristol, United Kingdom

[49]Cavendish Laboratory, University of Cambridge, Cambridge, United Kingdom

[50]Department of Physics, University of Warwick, Coventry, United Kingdom

[51]STFC Rutherford Appleton Laboratory, Didcot, United Kingdom

[52]School of Physics and Astronomy, University of Edinburgh, Edinburgh, United Kingdom

[53]School of Physics and Astronomy, University of Glasgow, Glasgow, United Kingdom

[54]Oliver Lodge Laboratory, University of Liverpool, Liverpool, United Kingdom

[55]Imperial College London, London, United Kingdom

[56]School of Physics and Astronomy, University of Manchester, Manchester, United Kingdom

[57]Department of Physics, University of Oxford, Oxford, United Kingdom

[58]Massachusetts Institute of Technology, Cambridge, MA, United States

[59]University of Cincinnati, Cincinnati, OH, United States

[60]University of Maryland, College Park, MD, United States

[61]Syracuse University, Syracuse, NY, United States

[62]Pontifícia Universidade Católica do Rio de Janeiro (PUC-Rio), Rio de Janeiro, Brazil, associated to [2]

[63]University of Chinese Academy of Sciences, Beijing, China, associated to [3]

[64]Institute of Particle Physics, Central China Normal University, Wuhan, Hubei, China, associated to [3]

[65]Departamento de Fisica , Universidad Nacional de Colombia, Bogota, Colombia, associated to [8]

[66]Institut für Physik, Universität Rostock, Rostock, Germany, associated to [12]

[67]National Research Centre Kurchatov Institute, Moscow, Russia, associated to [32]

[68]Instituto de Fisica Corpuscular (IFIC), Universitat de Valencia-CSIC, Valencia, Spain, associated to [38]

[69]Van Swinderen Institute, University of Groningen, Groningen, The Netherlands, associated to [43]

[a]Universidade Federal do Triângulo Mineiro (UFTM), Uberaba-MG, Brazil

[b]Laboratoire Leprince-Ringuet, Palaiseau, France

[c]P.N. Lebedev Physical Institute, Russian Academy of Science (LPI RAS), Moscow, Russia

[d]Università di Bari, Bari, Italy

[e]Università di Bologna, Bologna, Italy

[f]Università di Cagliari, Cagliari, Italy

[g]Università di Ferrara, Ferrara, Italy

[h] *Università di Genova, Genova, Italy*

[i] *Università di Milano Bicocca, Milano, Italy*

[j] *Università di Roma Tor Vergata, Roma, Italy*

[k] *Università di Roma La Sapienza, Roma, Italy*

[l] *AGH - University of Science and Technology, Faculty of Computer Science, Electronics and Telecommunications, Kraków, Poland*

[m] *LIFAELS, La Salle, Universitat Ramon Llull, Barcelona, Spain*

[n] *Hanoi University of Science, Hanoi, Viet Nam*

[o] *Università di Padova, Padova, Italy*

[p] *Università di Pisa, Pisa, Italy*

[q] *Università degli Studi di Milano, Milano, Italy*

[r] *Università di Urbino, Urbino, Italy*

[s] *Università della Basilicata, Potenza, Italy*

[t] *Scuola Normale Superiore, Pisa, Italy*

[u] *Università di Modena e Reggio Emilia, Modena, Italy*

[v] *Iligan Institute of Technology (IIT), Iligan, Philippines*